Journal Name

ARTICLE

Nanoscale Interfacial Electroactivity in PVDF/PVDF-TrFE Blended Films with Enhanced Dielectric and Ferroelectric Properties

Received 00th January 20xx,
Accepted 00th January 20xx

DOI: 10.1039/x0xx00000x

www.rsc.org/

Nan Meng,[a] Xiaojing Zhu,[a] Rui Mao,[a] Michael John Reece,[a] and Emiliano Bilotti[a]*

The typical limitations of ferroelectric polymers like poly (vinylidene fluoride) (PVDF) - low crystallinity, indirect ferroelectric β-phase crystallization - and poly (vinylidene fluoride-trifluoroethylene) (PVDF-TrFE) - higher material and processing costs, lower Curie point - are tackled by a simple and industrially viable melt blending approach. Despite the immiscible nature of PVDF and PVDF-TrFE, strong interactions exist between the two polymers, which substantially affects the morphology and texture of the blends as well as their dielectric and ferroelectric properties. Surprisingly, minor amounts of PVDF-TrFE lead to a significant increase in β-phase content and preferred orientation of PVDF, well beyond the rule-of-mixtures. Moreover, the blends exhibit maximum increases in dielectric constant of 80% and 30%, respectively, compared with pure PVDF and PVDF-TrFE. The ferroelectric remnant polarization increases from 0.040 to 0.077 C/m^2, while the coercive field decreases from 75 to 32 kV/mm with increasing PVDF-TrFE content from 0 to 40 wt. %. The enhancement of properties is explained by the strong interactions at the interfaces between PVDF and PVDF-TrFE, which also suppresses the Curie transition of PVDF-TrFE, providing a potentially increased working temperature range for blended films, which is important in applications like non-volatile energy storage devices, ferroelectric field-effect transistors and touch sensors.

Introduction

Polymer-based ferroelectric materials have low processing temperatures, high electrical resistivity and excellent flexibility compared to ceramic materials, which makes them of interest for flexible electronic devices, such as memories and sensors.[1-6] Poly (vinylidene fluoride) (PVDF) and its copolymers with trifluoethylene (PVDF-TrFE) can be easily fabricated into films with good ferroelectric properties. Unlike ferroelectric ceramics, whose polar properties originate from ion displacement inside the crystal unit cell, the polar properties of ferroelectric polymers are due to the polar groups in the crystalline polymer structure. As a consequence of this, the coercive field of ferroelectric polymers is high (> 50 kV/mm).[7]

PVDF, a semi-crystalline polymer, shows at least four polymorphs (α-, β-, γ- and δ-).[7] The crystallization from the melt normally leads to the non-polar α-phase, which possesses trans-gauche chain conformation resulting in the self-cancelation of the dipoles.[7] The α-phase PVDF can be transformed into the γ-phase through thermal treatments[8] and into the δ-phase through poling under high electric field (~ 150 kV/mm).[9, 10] While the γ and δ- phase are polar to some extent, the β-phase displays the best piezoelectric and ferroelectric properties. The polar direction of β-PVDF is along its b-axis, while the polymer chains are aligned with the c-axis.[7] β-phase PVDF can be made by mechanically stretching α-phase PVDF [11] or poling α- and δ-PVDF at even higher electric fields (> 500 kV/mm).[10]

On the other hand, the copolymer PVDF-TrFE with TrFE content in the range of 20-35 mol. % easily crystalizes as the ferroelectric β-phase, independent of the processing routes or post-treatments.[12] Moreover, the crystallinity of PVDF-TrFE is much higher compared with ~ 50% for PVDF, and can reach 90% after annealing in the temperature range between the Curie and melting points.[13] This is due to the increased chain mobility of PVDF-TrFE, leading to an increase in the lamella thickness. However, the large scale application of PVDF-TrFE is impeded by its time-consuming and expensive synthesis,[12] along with a limited working temperature range due to the existence of Curie transition.

Blending is a common strategy to modify the properties of a base polymer by combining the desirable characteristics of different polymers. Miscibility is an important issue related to the evaluation of blends. PVDF blends with amorphous polymers containing carbonyl group (e.g. poly methyl methacrylate PMMA) exhibit good miscibility in the whole composition range due to the contribution from the hydrogen bonding between the double-bonded oxygen of the carbonyl group and the acidic hydrogen of the CH_2-CF_2 group.[14-16] However, the crystallization of PVDF and its spontaneous polarization are suppressed with the addition of amorphous polymers.[15, 17] As a result, in order to maintain or even

[a] School of Engineering and Materials Science, Queen Mary University of London, Mile End Road, E1 4NS, UK, E-mail: e.bilotti@qmul.ac.uk

Electronic Supplementary Information (ESI) available: [details of any supplementary information available should be included here]. See DOI: 10.1039/x0xx00000x

Please do not adjust margins

enhance its ferroelectric properties, blending with fluorine polymers is more likely to be effective. [18]

Tanaka *et al.* [19] investigated the miscibility of PVDF/PVDF-TrFE blends. Based on the observation of two distinct fusion peaks in the DSC heating run, PVDF was found to be immiscible with PVDF-TrFE regardless of the composition of the copolymer. Gregorio *et al.* [20] came to the same conclusion, but they suggested that PVDF and PVDF-TrFE displayed miscibility on a lamellae level due to the fact that pure PVDF showed axial morphology, while the blends displayed homogenously distributed irregular texture, suggesting that PVDF-TrFE molecules segregated to the regions between the PVDF spherulites. However, they did not report the electric properties of their blended films. Despite the immiscibility of the polymers, there is evidence of strong interaction in PVDF/PVDF-TrFE blends, which might have a significant effect on the dielectric and ferroelectric properties of the blends.

In this work, PVDF was blended with PVDF-TrFE using melt extrusion, which, to the best of our knowledge, has never been reported before. On the basis of our previous study,[21] melt extruded PVDF-TrFE films exhibited remarkable ferroelectric properties due to high crystallinity and highly preferred crystalline orientation. It is proposed that the presence of PVDF-TrFE could enhance the crystallization of PVDF into β-phase and generate preferred orientation of its polymer chains.

Experimental

Materials

PVDF was purchased from Sigma Aldrich Chemical Co. The average molecular weight of the PVDF was about 180 kg/mol (Mw) and 71 kg/mol (Mn). PVDF-TrFE of composition 77/23 mol% was purchased from Piezotech S.A.S, (France). The average molecular weight of the PVDF-TrFE was 210 kg/mol (Mw) and 100 kg/mol (Mn).[22]

Sample preparation

PVDF and PVDF-TrFE were melt-blended using a DSM X'plore 15 Mini-extruder (Xplore Instruments, Geleen, The Netherlands), at 205 ℃ and 60 rpm for 10 min. The weight ratios of PVDF/PVDF-TrFE were set as 100/0, 90/10, 80/20, 70/30, 60/40 and 0/100. A slit die with gauge of 200 μm was used to produce films. The films were collected by a roller at 180 mm/min and ambient temperature. The films were then clamped and annealed at 100 ℃ for 2 hours. The thickness of the films was about 20 μm. For the electrical measurements, gold was vacuum sputtered on both sides of the films to form electrodes.

Instrumentation

Fourier transform infrared spectroscopy (FTIR) (Tensor 27, Bruker Optik GmbH, Ettlingen, Germany) was used to characterize the crystalline phases. Five specimens were characterized for every composition of film. To complement the FTIR data, the crystalline phases were also determined using one-dimensional wide-angle X-ray diffraction (1D-WAXD) patterns which were obtained using a Bragg-Brentano geometry X-ray diffractometer (X'Pert Pro, PANalytical, Almelo, The Netherlands) with Cu/Kα radiation in the 2θ range of 5°-70°. The preferred orientation of the films was determined using two-dimensional wide-angle X-ray diffraction (2D-WAXD) ring patterns, which were obtained using a transmission geometry X-ray diffractometer (Kappa ApexII Duo, Bruker AXS GmbH, Karlsruhe, Germany). The surface morphology of the films was studied using a scanning electron microscopy (SEM) (FEI Inspect-F, Hillsboro, OR, USA). Before gold coating, samples were etched in potassium permanganate solution for 40 min at 50 ℃ to remove the amorphous region. The thermal properties of the materials were analyzed using a differential scanning calorimeter (DSC) (DSC822e, Mettler-Toledo, OH, USA) under N_2 atmosphere. All of the samples were initially heated up to 180 ℃ and kept at this temperature for 5 min, then cooled down to 25 ℃ and heated up again to 180 ℃. Both the heating and cooling rates were set at 5 ℃/min. Isothermal crystallization was carried out at 150 ℃ and 135 ℃. The frequency dependence of dielectric permittivity and dielectric loss tangent were measured using a Precision Impedance Analyzer (4294A; Agilent, Santa Clara, CA) at ambient temperature in the frequency range of 100 Hz to 100 MHz with an applied maximum voltage of 0.5 V. The temperature dependence of dielectric permittivity and dielectric loss tangent were measured at different frequencies using a LCR meter (4284A; Agilent, Santa Clara, CA) which is connected with a homemade furnace. The electrode diameter for dielectric tests was 5 mm. The ferroelectric P-E hysteresis loops were tested using a ferroelectric hysteresis measurement tester (NPL, Teddington, UK) at ambient temperature and 10 Hz. The electrode diameter for ferroelectric tests was 2 mm. Both the dielectric and ferroelectric data presented in this paper was based on the testing of 8 different specimens.

Results and Discussions

Crystalline Phases and Preferred Orientation of PVDF/PVDF-TrFE Blended Films

The FTIR spectra of the blended films are shown in **Figure 1**a. For pure PVDF, the strong α-phase characteristic bands at 1211, 1179, 1145, 1066, 976, 871, 854, 795, 764 and 613 cm^{-1} can be seen in line (1). FTIR cannot clearly distinguish the β-from the γ-phase since several of their characteristic bands overlap.[23, 24] For example, the typical 840 cm^{-1} β-phase band could also be a superposition of bands for the β- and γ-phases.[24, 25] However, the exclusive γ-phase bands at 1234, 1117, 833 and 812 cm^{-1} are not apparent in line (1),[26] which means that only the β-phase contributed to the formation of the band at 840 cm^{-1}. To sum up, pure PVDF films mainly crystallized into the α-phase with a small amount of the β-phase (～ 8 wt. % as shown in **Figure 1**b).

This journal is © The Royal Society of Chemistry 20xx

Please do not adjust margins

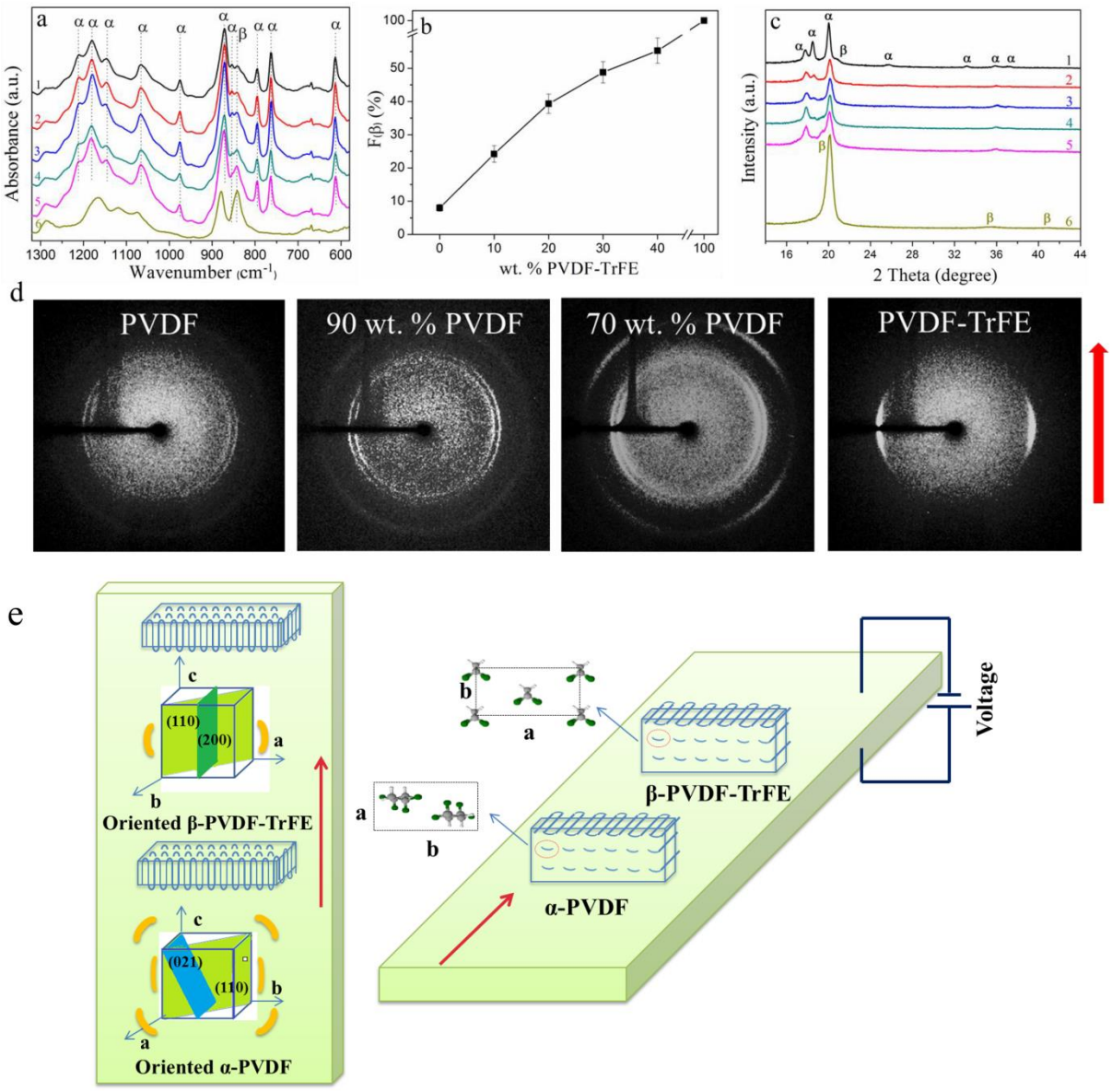

Figure 1. (a) FTIR spectra of: (1) PVDF/PVDF-TrFE 100/0; (2) PVDF/PVDF-TrFE 90/10 wt.%; (3) PVDF/PVDF-TrFE 80/20 wt.%; (4) PVDF/PVDF-TrFE 70/30 wt.%; (5) PVDF/PVDF-TrFE 60/40 wt.%; (6) PVDF/PVDF-TrFE 0/100; **(b)** F(β) of pure PVDF and blended films as a function of wt. % PVDF-TrFE; **(c)** 1D-WAXD of: (1) PVDF/PVDF-TrFE 100/0; (2) PVDF/PVDF-TrFE 90/10 wt.%; (3) PVDF/PVDF-TrFE 80/20 wt.%; (4) PVDF/PVDF-TrFE 70/30 wt.%; (5)PVDF/PVDF-TrFE 60/40 wt.%; (6) PVDF/PVDF-TrFE 0/100; **(d**) 2D-WAXD of PVDF, PVDF-TrFE and blends containing 90 wt. % and 70 wt. % PVDF; **(e)** schematic diagram illustrating the orientation of the blended films; the left reflects the film surface and can be used for the understanding of 2D-WAXD; the right reflects the cross-section region. The rectangles represent the lamellae with folded polymer chains. The red arrows indicate the extrusion direction.

For pure PVDF-TrFE, strong characteristic β-phase bands at 1167, 878 and 840 cm^{-1} can be seen in **Figure 1**a line (6). The blended films show a mixture of α- and β-phase. The intensity of the 854 cm^{-1} band (α-phase) was considerably reduced with increasing amount of PVDF-TrFE, while the 840 cm^{-1} band (β-phase) became more obvious. Equation 1 was used to quantify the relative fraction of the β-phase (F(β)), assuming that only the α- and β-phases existed.[27, 28] Equation 1 is built on the assumption that FTIR follows the Lambert-Beer law.[27] In Equation 1, A_α and A_β correspond to the measured absorbance at 764 cm^{-1} and 840 cm^{-1}, and K_α and K_β are the absorbance coefficients at 764 cm^{-1} and 840 cm^{-1}, the values of which are 6.1×10^4 and 7.7×10^4 cm^2mol^{-1}, respectively [27]. The values of F(β) for the blended films are shown in **Figure 1**b; the value of F(β) of PVDF and PVDF-TrFE are also included. The F(β) value increases to almost 40 wt. % for PVDF/PVDF-TrFE 80/20 wt. % blended films, which shows that the introduction of PVDF-TrFE promotes the crystallization of PVDF into the β-phase.

$$F(\beta) = \frac{A_\beta}{\left(\frac{K_\beta}{K_\alpha}\right)A_\alpha + A_\beta} \quad (1)$$

Figure 1c shows 1D-WAXD patterns for the pure PVDF, PVDF-TrFE, and the blended films. The three main peaks for

Please do not adjust margins

Please do not adjust margins

the pure PVDF films, at 2θ=17.82°, 18.48° and 20.05°, suggest that PVDF mainly crystallized into the α-phase, [10, 29-34] consistent with the FTIR data which shows no traces of the γ-phase but about 8 wt.% of the β-phase. The shoulder peak for PVDF at 2θ=20.08° also indicates the existence of a small amount of β-phase in pure PVDF films. For the pure PVDF-TrFE films, one strong (110)/(200) reflection peak at 2θ=20.12° was observed. Two other peaks at 2θ= 35.5° and 40.9° were extremely weak and broad, which indicates a high preferred orientation for the pure PVDF-TrFE films.[33]

Similar to PVDF, the blended films showed three XRD peaks. The intensity of the characteristic (020) α-PVDF peak at about 18.5° significantly reduced with PVDF-TrFE content, especially for the blended films containing more than 20 wt. % PVDF-TrFE. The weakening of this peak indicates that the amount of the α-phase was reduced and/or the preferred orientation of the crystallites increased with the presence of PVDF-TrFE. Combined with the FTIR data, it can be confirmed that there was a reduction in the α-phase and a corresponding increase in the β-phase PVDF.

The preferred orientation results for the PVDF and PVDF-TrFE films obtained from 2D-WAXD analysis are shown in **Figure 1**d. From inner to outer, the WAXD reflections of the PVDF, calculated from **Figure 1**d, are 18.1°, 20.0° and 26.6°. The ring at 18.1° consists of the overlapping 17.81° $(100)_\alpha$ and 18.48° $(020)_\alpha$ reflections. The reflection at 26.6°, though not obvious in **Figure 1**c, is associated with the $(021)_\alpha$ plane, which is characteristic of the α-phase. As clearly seen in **Figure 1**d, the crystalline phase of PVDF-TrFE is well oriented, with the $(110)_\beta/(200)_\beta$ reflections concentrated towards the equatorial region, indicating that the polymer chain axis (c-axis) is oriented parallel to the extrusion direction.[21] In comparison, the reflections of PVDF are more uniformly distributed, implying low preferred orientation. The orientation difference can be explained by the fact that PVDF-TrFE exhibits a longer relaxation time in the melt state than that of PVDF, and therefore showed a more pronounced crystal orientation during flow extension.[35]

The 2D-WAXD patterns for the blended films are shown in **Figure 1**d. From inner to outer, the WAXD profiles exhibit the characteristic reflections of $(100)_\alpha/(020)_\alpha$, $(110)_{\alpha+\beta}/(200)_\beta$ and $(021)_\alpha$ planes at 18.36°, 20.33° and 26.6° respectively. With increasing amount of PVDF-TrFE, the preferred orientation of the $(110)_{\alpha+\beta}/(200)_\beta$ and $(021)_\alpha$ reflections are enhanced. The intensity as a function of azimuthal angle from -90° to +90° at the radial position of the $(110)_{\alpha+\beta}/(200)_\beta$ and $(100)_\alpha/(020)_\alpha$ peak for the pure PVDF, PVDF-TrFE and blended films was fitted with a Gaussian function (**Figure S1**). Pure PVDF films show the least preferred orientation, corresponding to the broadest peak (**Figure S1**). For the blended films (**Figure S1**) the intensity is enhanced and the peak becomes sharper radially and azimuthally with increasing amount of PVDF-TrFE, which shows that blending with PVDF-TrFE leads to increased crystallinity and higher preferred orientation for the PVDF/PVDF-TrFE blended films. Interestingly, the outermost 26.6° $(021)_\alpha$ reflection ring of the blended films shows preferred orientation, about 45° from the equatorial direction, which enhanced with increasing the amount of PVDF-TrFE (**Figure 1**d). During extrusion, the temperature dropped quickly from 205 ℃ to room temperature, which caused the PVDF and PVDF-TrFE to crystallize simultaneously. The existence of a strong interaction between the two different polymers caused the chains of the PVDF to orientate in the same direction as the PVDF-TrFE. **Figure 1**e depicts the orientation of the blended films formed during the extrusion processing.

Miscibility and crystallization behavior of PVDF/PVDF-TrFE blended films

Morphology studies

It is known that PVDF crystallizes as spherulites when prepared by melt processing,[7] while PVDF-TrFE crystallizes with stacked lamellae structure.[36] **Figure 2**a-b shows the surface morphology of the PVDF and PVDF-TrFE films. The arrow in **Figure 2** indicates the extrusion direction. For PVDF, the lamellae tend to form spherulites with little preferred orientation, while PVDF-TrFE displays a stacked lamellar morphology.[37]. For the blended films, the two components crystallize together without obvious phase separation (**Figure 2**c-f). Furthermore, the introduction of PVDF-TrFE produces distortion of the spherulites as can be seen in **Figure 2**f for the PVDF/PVDF-TrFE 60/40 wt. % blended film.

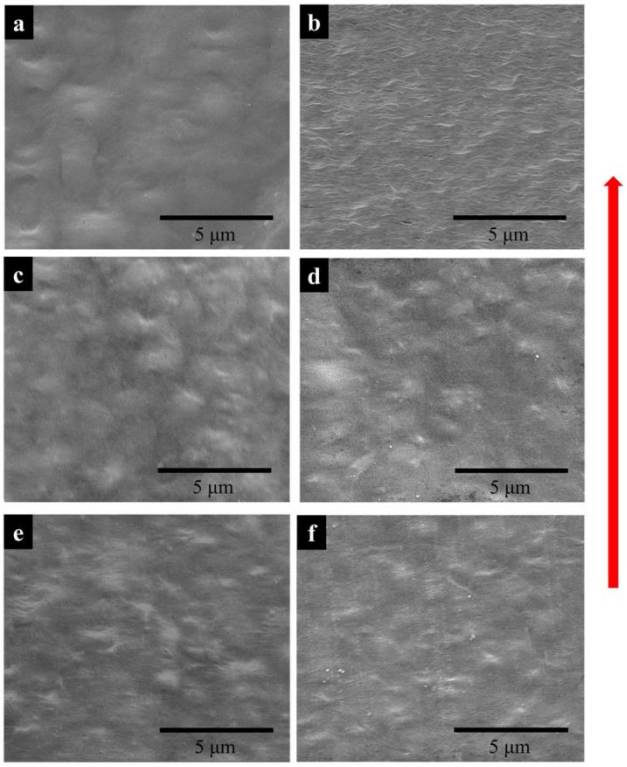

Figure 2. SEM of surfaces of: **(a)** PVDF; **(b)** PVDF-TrFE; **(c)** PVDF/PVDF-TrFE 90/10 wt. %; **(d)** PVDF/PVDF-TrFE 80/20 wt. %; **(e)** PVDF/PVDF-TrFE 70/30 wt. %; **(f)** PVDF/PVDF-TrFE 60/40 wt. % (arrow indicates extrusion direction).

Thermal analysis

Figure 3 shows the DSC scans of PVDF, PVDF-TrFE and their blends. The first heating curves are displayed in **Figure 3**a. Pure

 This journal is © The Royal Society of Chemistry 20xx

Please do not adjust margins

Please do not adjust margins

PVDF has two obvious fusion peaks at 161.3±0.3 ℃ and 169.9±0.4 ℃, which could be caused by the existence of different crystalline phases or crystallization imperfection. The melting endotherms of α- and β-PVDF are reported to be at almost the same position, both at around 167 ℃.[27] Combined with the FTIR results for PVDF, it can be deduced that the 169.9 ℃ endotherm peak corresponds to the melting of the well-formed prevalent α-phase crystals, while the 161.3 ℃ peak can be attributed to the melting of imperfect crystalline regions.[38, 39] It is seen in Table 1 that pure PVDF exhibits a fusion enthalpy (ΔH_f) of 43.1 J/g, indicating the crystallinity of the pure PVDF extruded films is about 41% (ΔH_f for 100% crystalline PVDF is 104.6 J/g[40]).

Apart from its fusion peak at 147.2±0.2 ℃, pure PVDF-TrFE shows another peak at 133.8±0.1 ℃ originating from the ferroelectric to paraelectric phase transition (Curie transition). The ΔH_f of PVDF-TrFE is 29.0 J/g, suggesting a crystallinity of 76% (ΔH_f for 100% crystalline PVDF-TrFE is about 38 J/g[41]). The blended films exhibit three peaks on first heating, corresponding to the fusion peaks for PVDF-TrFE and PVDF, which proves the immiscibility of the two polymers. Interestingly, the Curie transition peak for PVDF-TrFE is diffuse and is apparent only as a shoulder on the lower temperature side of the fusion peak of PVDF-TrFE.

Figure 3b shows the cooling DSC curves on cooling after first heating. Pure PVDF has one crystallization peak at 150.6±0.5 ℃ and pure PVDF-TrFE shows two peaks at 134.6±0.8 ℃ and 77.8±0.5 ℃, resulting from the crystallization and the paraelectric to ferroelectric phase transition, respectively. All blended films exhibit three peaks. The crystallization temperatures of PVDF and PVDF-TrFE and the Curie transition in the blended films are slightly lower than those of the pure components.

Figure 3c shows the second heating DSC curves of PVDF, PVDF-TrFE and their blends. During the second heating pure PVDF has two fusion peaks at 168.9±0.3 ℃ and 174.8±0.2 ℃, indicating a mixture of α- and γ-phases.[23] Further evidence for the presence of the γ-phase can be found in the FTIR data presented in **Figure S2**. With regard to pure PVDF-TrFE, the peak value of the Curie transition shifts to a lower temperature (127±0.1 ℃) when compared to the first heating (133.8±0.1 ℃). The higher Curie point in the first heating indicates that the pure PVDF-TrFE crystallized into highly oriented ferroelectric crystals through the extrusion method.[42] For the blended films, the Curie transition peak was diffuse in the first heating curves, however, a small, but clear, peak can be seen in the second heating curves. It is shown in Table 1 that $\Delta H_{f\ PVDF}$ of pure PVDF and blended samples during first heating are larger than those of second heating, while being lower for $\Delta H_{f\ PVDF\text{-}TrFE}$, which indicates the existence of interactions between PVDF and PVDF-TrFE in the extruded blended films. PVDF crystallized first and served as a nucleating agent in the crystallization of PVDF-TrFE. The formed crystallites exhibited similar structure and were intimately correlated. The Curie transition is achieved by the formation of gauche bonds, which requires the polymer chains in PVDF-TrFE to undergo severe twisting and/or tilting[42], which needs adequate space to accomplish this. However, the surrounding PVDF crystals and the intimate coexistence of the two components restrict the space to accomplish the transition. However, PVDF and PVDF-TrFE crystallized more freely during the DSC slow cooling process (cooling rate 5 ℃/min), which resulted in more phase separation and less interactions, making the Curie transition peaks more obvious than those of the extruded blended films in the first DSC heating curves.

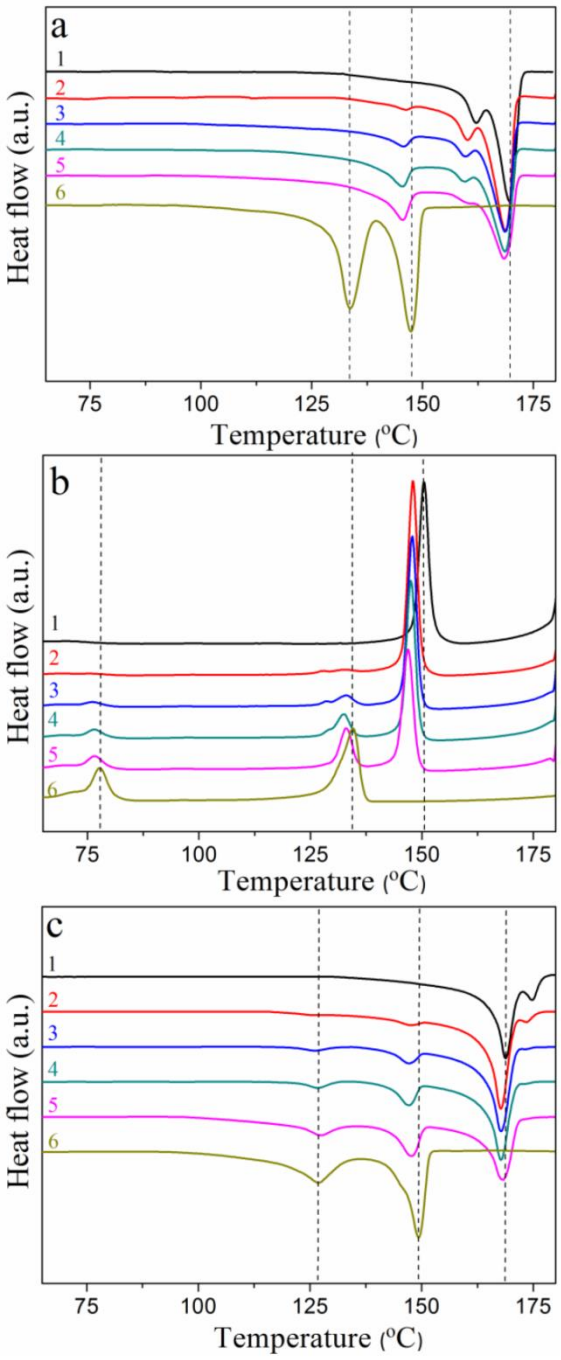

Figure 3. (a) First heating; **(b)** cooling; and **(c)** second heating DSC graphs of: (1) PVDF/PVDF-TrFE 100/0; (2) PVDF/PVDF-TrFE 90/10 wt.%; (3) PVDF/PVDF-TrFE 80/20 wt.%; (4) PVDF/PVDF-TrFE 70/30 wt.%; (5) PVDF/PVDF-TrFE 60/40 wt.%; (6) PVDF/PVDF-TrFE 0/100.

Please do not adjust margins

Please do not adjust margins

Table 1 The enthalpy of Curie transition and fusion of PVDF/PVDF-TrFE blended films acquired from first heating and second heating DSC curves.

PVDF/ PVDF-TrFE	Enthalpy values of first heating (J/g)			Enthalpy values of second heating (J/g)		
	[a] $\Delta H_{c\ PVDF\text{-}TrFE}$	$\Delta H_{f\ PVDF\text{-}TrFE}$	$\Delta H_{f\ PVDF}$	$\Delta H_{c\ PVDF\text{-}TrFE}$	$\Delta H_{f\ PVDF\text{-}TrFE}$	$\Delta H_{f\ PVDF}$
100/0	–	–	46.3±3	–	–	43.1±2
90/10	–	7.0±1	38.0±2	9.2±1	13.1±1	31.1±1
80/20	–	6.6±1	36.4±3	9.0±1	13.6±1	32.7±1
70/30	–	17.1±2	33.0±3	7.8±1	19.6±1	32.0±1
60/40	–	15.6±1	32.5±2	12.2±2	21.0±1	31.9±1
0/100	28.7±2	29.0±3	–	26.4±3	28.8±2	–

[a] $\Delta H_{c\ PVDF\text{-}TrFE}$: enthalpy of Curie transition of PVDF-TrFE; $\Delta H_{f\ PVDF\text{-}TrFE}$ and $\Delta H_{f\ PVDF}$: fusion enthalpy of PVDF-TrFE and PVDF, respectively.

The above results correlated to both crystallization and morphological studies strongly demonstrate the intimate interactions between the PVDF and PVDF-TrFE. More detailed investigations of isothermal crystallization at 150 °C (PVDF crystallization temperature) and 135 °C (PVDF-TrFE crystallization temperature) were undertaken.

The DSC data recorded during isothermal crystallization at 150 °C is shown in **Figure 4**a and **Figure S3**, and the morphology of the films is shown in **Figure 5**a. No crystallization of PVDF-TrFE occurred at 150 °C (**Figure S3**). It is evident that the rate of crystallization of the PVDF at 150 °C was increased by the addition of PVDF-TrFE (in melt state). This is different to what is reported for PVDF/poly(1,4-butylene adipate) (PBA) blends where the crystallization rate of PVDF was reduced due to the presence of PBA.[43] To understand these differences, it is necessary to consider the morphologies of the microstructures. In the PVDF/PBA system, PVDF crystallized into progressively larger spherulites with increasing PBA content, however, in our PVDF/PVDF-TrFE blends the growth of PVDF spherulites was restricted. The isothermally crystallized PVDF showed fine spherulites. The spherulites that formed in the blended samples were smaller and less perfect compared to those in PVDF (**Figure 5**a), which is consistent with the morphology of extruded films. On the basis that there was no crystallization of PVDF-TrFE at 150 °C because the temperature was above its melting point, the crystallization enthalpy of the blends were normalized in terms of the PVDF content ($\Delta H_{c/PVDF}$). **Figure 4**a shows that the normalized values of $\Delta H_{c/PVDF}$ for both pure PVDF and the blends are similar regardless of weight ratio, indicative of almost no hindrance to the degree of crystallinity of PVDF due to the introduction of PVDF-TrFE.

The non-normalized raw DSC data for samples isothermally crystallized at 135 °C are shown in **Figure 4**b and **Figure S3** Pure PVDF-TrFE exhibited a maximum ΔH_c of approximately 37 J/g, which represents almost complete crystallization using the reported enthalpy for 100 % crystalline PVDF-TrFE (～38 J/g).[41] During the isothermal crystallization at 135 °C, the PVDF continued to crystallize as demonstrated by the large enthalpies of the blends. On the other hand, the rate of crystallization at 135 °C of the PVDF-TrFE was increased in the blends compared to the pure copolymer. This can be explained by the PVDF crystallites acting as nucleation sites for the crystallization of the PVDF-TrFE. **Figure 5**b shows the morphology of samples isothermally crystallized at 135 °C, with needle-like PVDF-TrFE crystals embedded in the matrix of PVDF, which did not crystallize into a spherulitic structure. To conclude, the DSC data (Figures 3, 4 and Table 1) and the microstructural analysis (Figures 2, and 5) clearly shows that synergistic effects occurred at the nanoscale in the blended materials at the interface between the two immiscible polymers that strongly affected the kinetics of crystallization and the microstructures that formed.

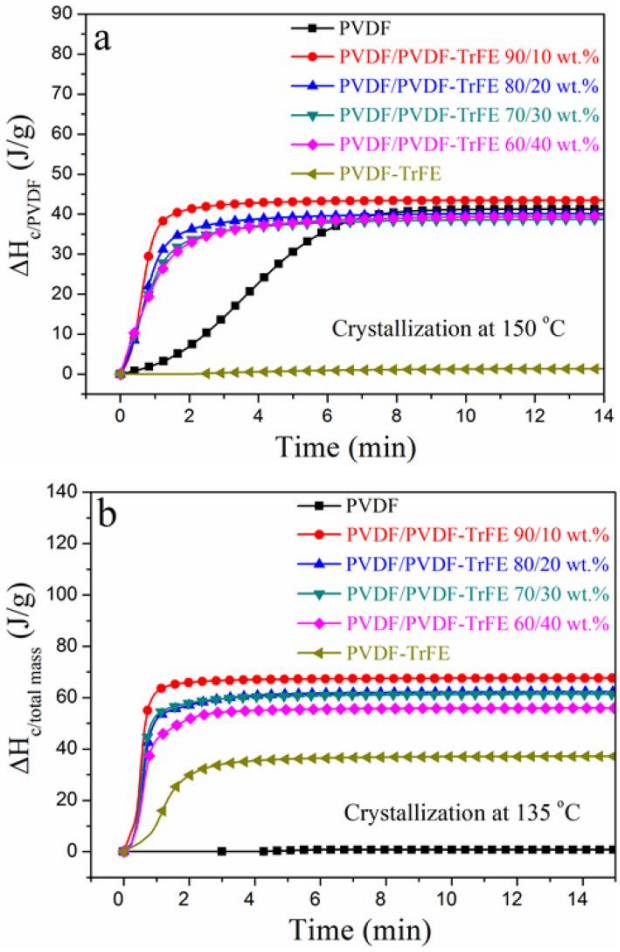

Figure 4. Crystallization enthalpy (ΔH_c) acquired by integrating heat flow recorded during isothermal crystallization as a function of time at: **(a)** 150 °C and **(b)** 135 °C. The ΔH_c values at 150 °C for blends materials were normalized by PVDF.

This journal is © The Royal Society of Chemistry 20xx

Please do not adjust margins

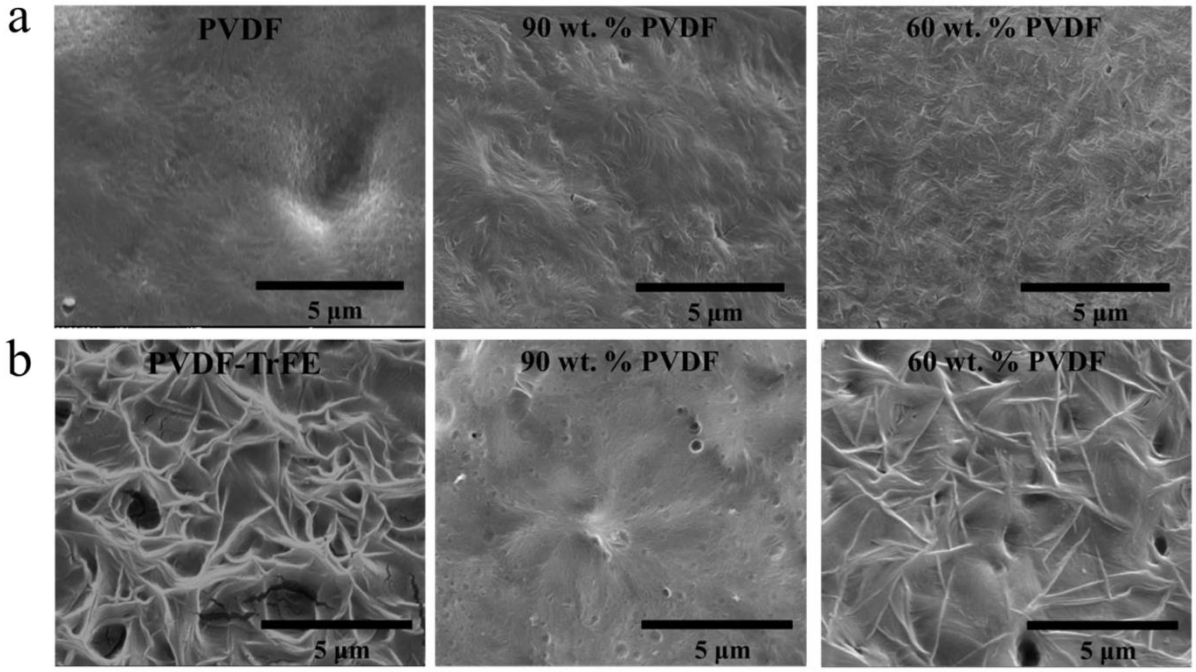

Figure 5. SEM morphology images for samples isothermally crystallized at **(a)** 150 °C and **(b)** 135 °C.

Electric properties of PVDF/PVDF-TrFE Blended Films

Dielectric properties

Figure 6a-b shows the frequency dependence of the dielectric permittivity and loss of PVDF, PVDF-TrFE and their blends. The blended films show larger dielectric constant values than those of the two pure components. One explanation for this could be enhanced interfacial polarization at the PVDF and PVDF-TrFE interfaces. Another possible explanation might be the preferred orientation of the polymer chains in the amorphous region, especially at the crystalline-amorphous interfaces.[44] The addition of PVDF-TrFE in the blended films increased the crystalline preferred orientation of the PVDF, thus causing the chains in the amorphous region to orient along the same direction, which gives rise to higher dielectric constant values than for pure PVDF.

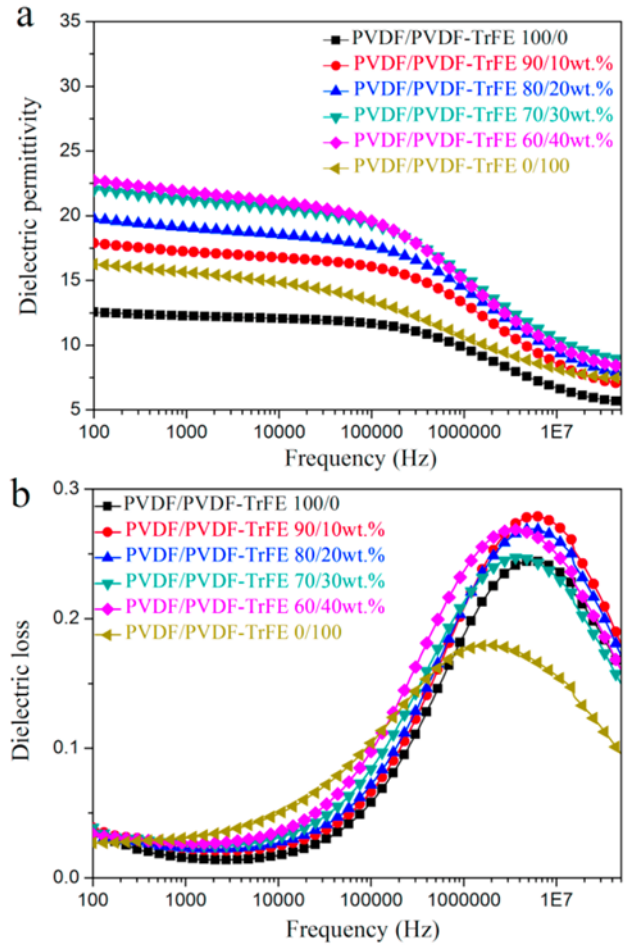

Figure 6. Frequency dependence of **(a)** dielectric permittivity and **(b)** dielectric loss for pure PVDF, PVDF-TrFE and blended films as a function of frequency.

Please do not adjust margins

Figure 7 shows the temperature dependent dielectric spectra for pure PVDF, PVDF-TrFE and their blends. All of the samples exhibit a dielectric loss peaks at about 0 °C, which is ascribed to the relaxation of the polymer chains in the amorphous regions (glass transition).[5] The dielectric permittivity of PVDF-TrFE shows an obvious peaks at about 140 °C, and the peak position is frequency invariant, which suggests the existence of Curie transition. [45] The blended films with 40 wt. % PVDF-TrFE show an inflexion in the permittivity and loss data consistent with a Curie transition (**Figure 7**c).

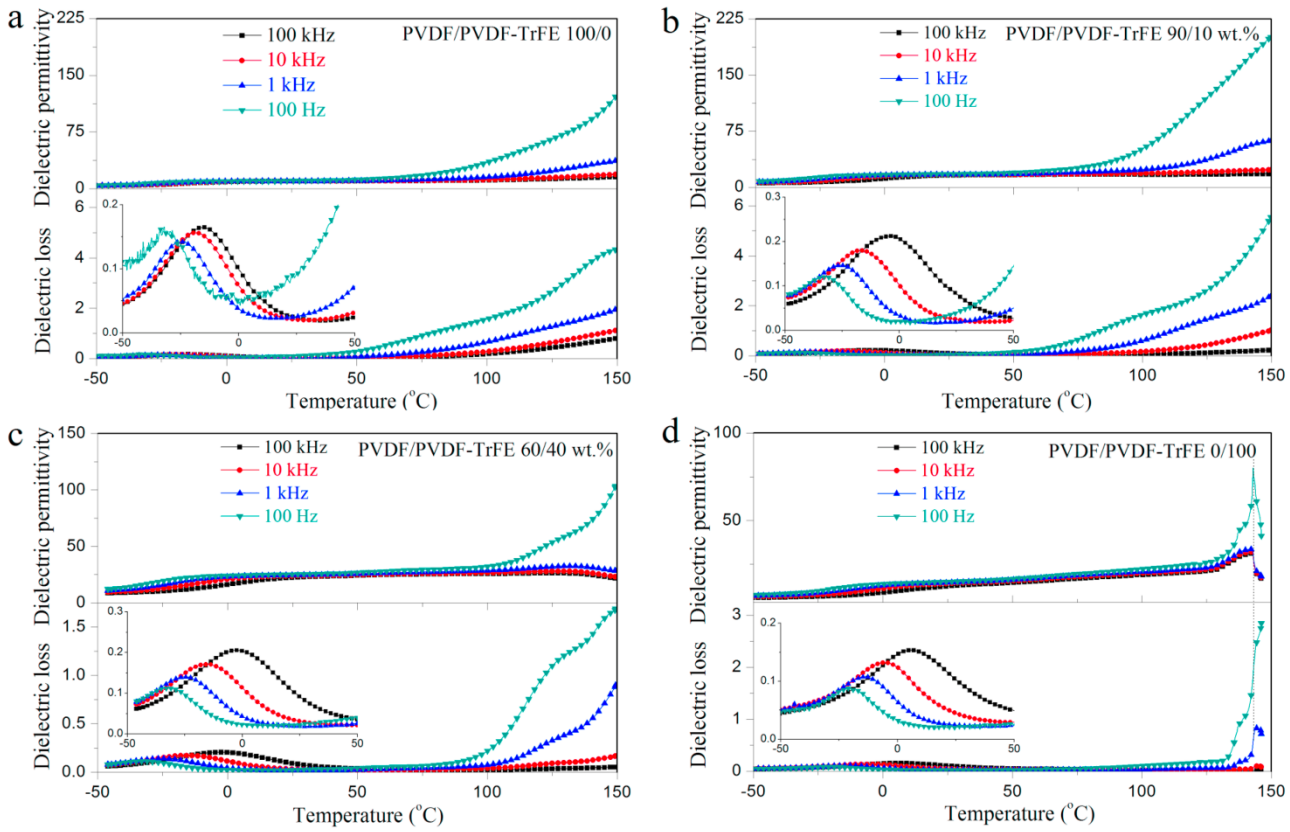

Figure 7. Temperature dependence of the dielectric permittivity and loss of: **(a)** PVDF; **(b)** PVDF/PVDF-TrFE 90/10 wt. %; **(c)** PVDF/PVDF-TrFE 60/40 wt. %; **(d)** PVDF-TrFE.

Ferroelectric properties

Figure 8 shows the ferroelectric polarization hysteresis loops for PVDF, PVDF-TrFE and the blended films. The P-E loops are saturated, which was confirmed by the invariance of the current peak position beyond a certain maximum applied electric field (~ 120 kV/mm). The PVDF-TrFE exhibits good ferroelectric properties, with a coercive field of about 35 kV/mm and a remnant polarization of 0.09 C/m^2, which is attributed to its highly preferred crystalline orientation and high crystallinity.[21] In the case of PVDF, a ferroelectric response was observed, confirmed by the presence of weak current peaks. The ferroelectric behavior of PVDF is attributed to the presence of the small amount of β-phase (~8 wt. %) and the transformation of the paraelectric α-phase to the ferroelectric δ-phase during the measurement.

With regard to the blended films, the coercive field decreased from 83 kV/mm to 32 kV/mm with increasing amount of PVDF-TrFE from 10 wt. % to 40 wt. % as a result of blending. The remnant polarization of the PVDF is apparently higher compared with 10 wt. % PVDF-TrFE due to the leakage current in the pure PVDF, making the remnant polarization of PVDF unrealistically high (inset in **Figure 8**a). Such leakage currents could be ascribed to the gaps or voids formed between large PVDF spherulites.[46] The introduction of PVDF-TrFE enhanced the remnant polarization for the blended films from 0.030 to 0.077 C/m^2 with increasing the amount of PVDF-TrFE from 10 to 40 wt. % (**Figure 8**c). On the basis of the data from the structural characterization, the addition of PVDF-TrFE enhanced the crystallization of ferroelectric β-phase in the blended films. This alone would not explain the enhanced ferroelectric properties of the blended films.

The theoretical value of the remnant polarization for the blended film with 40 wt. % copolymer based on the simple mixing rule was calculated using following equation: $P_{r\text{blends}} = \varphi_{\text{PVDF}} \times P_{r\text{PVDF}} + \varphi_{\text{PVDF-TrFE}} \times P_{r\text{PVDF-TrFE}}$, where φ and P_r are the volume fraction and measured remnant polarization for pure PVDF and PVDF-TrFE extruded samples. The calculated value for the blended film with 40 wt. % copolymer is only 0.058 C/m^2, about 25% lower than the experimental value. Similar conditions existed in the 20 wt. % and 30 wt. % blends, where the calculated values were about 20% less compared with the experimental values. Combined with the diffuse Curie transition and larger dielectric constants observed for the blended films, the interaction between the two polymers and the interfaces between them could explain the enhanced ferroelectric properties of the blended films. The interfacial

Please do not adjust margins

polarization contributed to the higher remnant polarization and more contributions were generated at high electric fields, as indicated by the large saturated polarization of blends with 40 wt. % PVDF-TrFE.

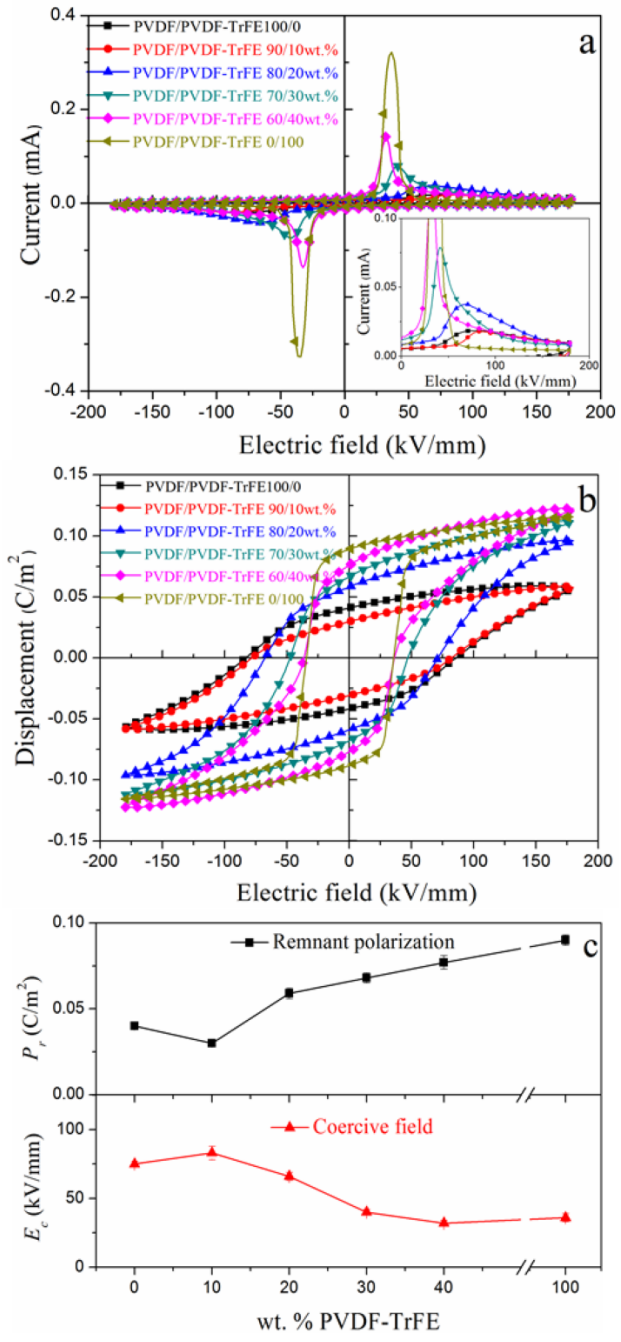

Figure 8. Ferroelectric properties of: (1) PVDF/PVDF-TrFE 100/0; (2) PVDF/PVDF-TrFE 90/10 wt.%; (3) PVDF/PVDF-TrFE 80/20 wt.%; (4) PVDF/PVDF-TrFE 70/30 wt.%; (5) PVDF/PVDF-TrFE 60/40 wt.%; (6) PVDF/PVDF-TrFE 0/100: (a) Current-Electric field I-E curves; (b) Polarization-Electric field P-E loops; (c) variations of remnant polarization P_r and switching field E_c as a function of wt. % PVDF-TrFE (data collected at E=180 kV/mm).

Conclusions

Despite the immiscibility of PVDF and PVDF-TrFE, as demonstrated by the DSC results, they intimately crystallize on a fine scale (~ 40 nm) without the appearance of distinct phase separation. The rate of crystallization of PVDF and PVDF-TrFE is increased as a result of blending, as suggested by isothermal crystallization studies. With increasing amount of PVDF-TrFE, the blended films have more β-phase and increased preferred orientation, more than would be expected based on a simple rule of mixtures. Due to interfacial polarization, PVDF/PVDF-TrFE blended films have larger dielectric constant than those of the two pure components. Furthermore, the ferroelectric properties of the blended films were enhanced more than would be expected based on a simple rule of mixtures. The switching field decreases (from 75 to 32 kV/mm), while the remnant polarization increases (from 0.040 to 0.077 C/m^2) with increasing amount of PVDF-TrFE from 0 to 40 wt. %. The Curie transition was suppressed in the blended films, which may lead to increased high temperature stability for piezoelectric applications.

Acknowledgements

We appreciate the valuable discussion with Prof *Cees Bastiaansen* and Prof *Ton Peijs*. *Nan Meng* is financially supported by the China Scholarship Council (CSC). Prof *Mike Reece* would also like to acknowledge the support of The Engineering and Physical Sciences Research Council (EP/L017695/1, MASSIVE).

Notes and references

1. Y. Yuan, T. J. Reece, P. Sharma, S. Poddar, S. Ducharme, A. Gruverman, Y. Yang and J. Huang, *Nat Mater*, 2011, **10**, 296-302.
2. M. Li, I. Katsouras, C. Piliego, G. Glasser, I. Lieberwirth, P. W. M. Blom and D. M. de Leeuw, *Journal of Materials Chemistry C*, 2013, **1**, 7695-7702.
3. B. Li, C. Xu, F. Zhang, J. Zheng and C. Xu, *Journal of Materials Chemistry C*, 2015, **3**, 8926-8931.
4. A. V. Shirinov and W. K. Schomburg, *Sensors and Actuators A: Physical*, 2008, **142**, 48-55.
5. L. Zhu, *The Journal of Physical Chemistry Letters*, 2014, **5**, 3677-3687.
6. Q. Li and Q. Wang, *Macromolecular Chemistry and Physics*, 2016, **217**, 1228-1244.
7. A. J. Lovinger, *Science*, 1983, **220**, 1115-1121.
8. W. M. Prest and D. J. Luca, *J Appl Phys*, 1978, **49**, 5042-5047.
9. N. C. Banik, P. L. Taylor and A. J. Hopfinger, *Appl Phys Lett*, 1980, **37**, 49-50.
10. G. T. Davis, J. E. McKinney, M. G. Broadhurst and S. C. Roth, *J Appl Phys*, 1978, **49**, 4998-5002.
11. K. Matsushige, K. Nagata, S. Imada and T. Takemura, *Polymer*, 1980, **21**, 1391-1397.
12. T. Furukawa, *Advances in Colloid and Interface Science*, 1997, **71–72**, 183-208.
13. O. Hiroji, A. Shuyo and K. Keiko, *Japanese Journal of Applied Physics*, 1988, **27**, 2144.
14. N. Tsutsumi, Y. Ueda, T. Kiyotsukuri, A. S. DeReggi and G. T. Davis, *J Appl Phys*, 1993, **74**, 3366-3372.

Please do not adjust margins

15. Q. Meng, W. Li, Y. Zheng and Z. Zhang, *J Appl Polym Sci*, 2010, **116**, 2674-2684.
16. Y. Tang and J. Scheinbeim, *Journal of Polymer Science Part B: Polymer Physics*, 2003, **41**, 927-935.
17. M. Li, N. Stingelin, J. J. Michels, M.-J. Spijkman, K. Asadi, K. Feldman, P. W. M. Blom and D. M. de Leeuw, *Macromolecules*, 2012, **45**, 7477-7485.
18. X. Zhang, Y. Shen, Z. Shen, J. Jiang, L. Chen and C.-W. Nan, *ACS Applied Materials & Interfaces*, 2016, **8**, 27236-27242.
19. H. Tanaka, A. J. Lovinger and D. D. Davis, *Journal of Polymer Science Part B: Polymer Physics*, 1990, **28**, 2183-2198.
20. R. Gregorio, M. R. Chaud, W. Nunes Dos Santos and J. B. Baldo, *J Appl Polym Sci*, 2002, **85**, 1362-1369.
21. N. Meng, R. Mao, W. Tu, X. Zhu, R. M. Wilson, E. Bilotti and M. J. Reece, *Polymer*, 2016, **100**, 69-76.
22. N. Shingne, M. Geuss, B. Hartmann-Azanza, M. Steinhart and T. Thurn-Albrecht, *Polymer*, 2013, **54**, 2737-2744.
23. R. Gregorio, *J Appl Polym Sci*, 2006, **100**, 3272-3279.
24. M. Li, H. J. Wondergem, M.-J. Spijkman, K. Asadi, I. Katsouras, P. W. M. Blom and D. M. de Leeuw, *Nat Mater*, 2013, **12**, 433-438.
25. R. Gregorio and R. C. CapitãO, *J Mater Sci*, 2000, **35**, 299-306.
26. J. H. Park, N. Kurra, M. N. AlMadhoun, I. N. Odeh and H. N. Alshareef, *Journal of Materials Chemistry C*, 2015, **3**, 2366-2370.
27. J. R. Gregorio and M. Cestari, *Journal of Polymer Science Part B: Polymer Physics*, 1994, **32**, 859-870.
28. M. P. Silva, V. Sencadas, G. Botelho, A. V. Machado, A. G. Rolo, J. G. Rocha and S. Lanceros-Mendez, *Materials Chemistry and Physics*, 2010, **122**, 87-92.
29. M. Sharma, G. Madras and S. Bose, *Physical Chemistry Chemical Physics*, 2014, **16**, 14792-14799.
30. Y. Takahashi and H. Tadokoro, *Macromolecules*, 1980, **13**, 1317-1318.
31. J. Buckley, P. Cebe, D. Cherdack, J. Crawford, B. S. Ince, M. Jenkins, J. Pan, M. Reveley, N. Washington and N. Wolchover, *Polymer*, 2006, **47**, 2411-2422.
32. D. M. Esterly and B. J. Love, *Journal of Polymer Science Part B: Polymer Physics*, 2004, **42**, 91-97.
33. J. L. Lutkenhaus, K. McEnnis, A. Serghei and T. P. Russell, *Macromolecules*, 2010, **43**, 3844-3850.
34. F. Oliveira, Y. Leterrier, J.-A. Månson, O. Sereda, A. Neels, A. Dommann and D. Damjanovic, *Journal of Polymer Science Part B: Polymer Physics*, 2014, **52**, 496-506.
35. P. K. Agarwal, R. H. Somani, W. Weng, A. Mehta, L. Yang, S. Ran, L. Liu and B. S. Hsiao, *Macromolecules*, 2003, **36**, 5226-5235.
36. C. M. Costa, M. N. T. Machiavello, J. L. G. Ribelles and S. Lanceros-Méndez, *J Mater Sci*, 2013, **48**, 3494-3504.
37. H. Zhou and G. L. Wilkes, *J Mater Sci*, 1998, **33**, 287-303.
38. D. R. Dillon, K. K. Tenneti, C. Y. Li, F. K. Ko, I. Sics and B. S. Hsiao, *Polymer*, 2006, **47**, 1678-1688.
39. J. Liu, X.-L. Lu and C.-R. Wu, *J Appl Polym Sci*, 2013, **129**, 1417-1425.
40. C. Marega and A. Marigo, *Eur Polym J*, 2003, **39**, 1713-1720.
41. O. Hiroji and K. Keiko, *Japanese Journal of Applied Physics*, 1982, **21**, L455.
42. K. Tashiro and M. Kobayashi, *Phase Transit*, 1989, **18**, 213-246.
43. J. P. Penning and R. St. John Manley, *Macromolecules*, 1996, **29**, 84-90.
44. L. Yang, J. Ho, E. Allahyarov, R. Mu and L. Zhu, *ACS Applied Materials & Interfaces*, 2015, **7**, 19894-19905.
45. H. Yan, H. Zhang, R. Ubic, M. J. Reece, J. Liu, Z. Shen and Z. Zhang, *Advanced Materials*, 2005, **17**, 1261-1265.
46. V. Cauda, S. Stassi, K. Bejtka and G. Canavese, *ACS Applied Materials & Interfaces*, 2013, **5**, 6430-6437.

1

This journal is © The Royal Society of Chemistry 20xx

Please do not adjust margins